

# Galaxy-CMB Cross-Correlation as a Probe of Alternative Models of Gravity

Fabian Schmidt<sup>1,2</sup>, Michele Liguori<sup>3</sup>, Scott Dodelson<sup>4,1,2</sup>

<sup>1</sup>*Department of Astronomy & Astrophysics, The University of Chicago, Chicago, IL 60637-1433*

<sup>2</sup>*Kavli Institute for Cosmological Physics, Chicago, IL 60637-1433*

<sup>3</sup>*Department of Applied Mathematics and Theoretical Physics,  
Centre for Mathematical Sciences, University of Cambridge,  
Wilberforce Road, Cambridge, CB3 0WA, United Kingdom and*

<sup>4</sup>*Center for Particle Astrophysics, Fermi National Accelerator Laboratory, Batavia, IL 60510-0500*

(Dated: February 6, 2020)

Bekenstein’s alternative to general relativity, TeVeS, reduces to Modified Newtonian Dynamics (MOND) in the galactic limit. On cosmological scales, the (potential well↔overdensity) relationship is quite different than in standard general relativity. Here we investigate the possibility of cross-correlating galaxies with the cosmic microwave background (CMB) to probe this relationship. At redshifts of order 2, the sign of the CMB-galaxy correlation differs in TeVeS from that in general relativity. We show that this effect is detectable and hence can serve as a powerful discriminator of these two models of gravity.

## I. INTRODUCTION

The standard theory of gravity, general relativity (GR), coupled with the standard model of particle physics cannot account for many cosmological observations, ranging from the dynamics of stars in galaxies to the large scale expansion of the universe. This discrepancy may well be resolved by adding to the standard model of particle physics. For example, dark matter in the form of supersymmetric particles could account for flat rotation curves and the large scale structure in the universe. Dark energy in the form of a cosmological constant or a scalar field could explain the acceleration of the universe. This scenario is commonly called the “ $\Lambda$ CDM model”.

Alternatively, general relativity may be wrong. Perhaps the theory needs to be modified on large scales to account for cosmological observations. Many attempts have been made along these lines [1–7], to explain either (or sometimes both) the acceleration of the universe and the phenomena usually associated with dark matter. One such attempt is Modified Newtonian Dynamics (MOND) initially proposed [8] to explain flat rotation curves in galaxies. Bekenstein [9] has recently introduced TeVeS, a theory which reduces to MOND in the appropriate limit but is robust enough to make predictions in many different arenas.

Several groups [10–13] have now studied the evolution of cosmic structure in TeVeS and the theory seems to be holding up. In some senses, this is surprising [14] since any no-dark matter theory faces the significant hurdle of explaining why the density field has gone nonlinear. Observations of the cosmic microwave background (CMB) pin down the baryon inhomogeneities at recombination to one part in  $10^4 - 10^5$ , and in standard general relativity, these inhomogeneities grow by only a factor of a thousand from that epoch until today.

As shown in [12], overdensities in TeVeS grow faster than in standard general relativity (GR). The mechanics of this is subtle: the vector field in TeVeS develops an instability and this growth in turn sources a difference between the two Newtonian scalar potentials. The two potentials  $\Phi$  and  $\Psi$  characterize scalar perturbations to the metric:

$$ds^2 = -dt^2 [1 + 2\Psi] + a^2(t) d\mathbf{x}^2 [1 + 2\Phi]. \quad (1)$$

In  $\Lambda$ CDM with standard GR, these two potentials are nearly equal to one another, so the TeVeS situation of unequal potentials is unfamiliar territory. In particular, the relation between gravitational potential and overdensity is quite different than in standard GR. Fig. 1 illustrates this.

In this paper, we demonstrate that one can test this prediction of TeVeS (for a different test, see [15]) by cross-correlating a deep galaxy survey with the CMB. A number of groups have already succeeded in cross-correlating tracers of the density field with the CMB [16–19]. The non-zero correlation is a result of the time-dependent gravitational potentials at late times because the universe is not completely matter dominated. In TeVeS, the potentials are determined not only by the matter overdensities but also by the behavior of the vector field. So the pattern of the cross-correlation changes. Most strikingly, at redshift of order 2–3 the cross-correlation changes sign. Observations of such a sign change would be a smoking gun signature of a modification of gravity.

Before proceeding with the calculation, we note that we focus on TeVeS as a fairly well-defined test model. Bertschinger [20] has pointed out however that generic modifications of gravity lead to changes of the sort discussed here. So we expect the cross-correlations envisioned here to be powerful tools cosmologists will use to discriminate (general relativity + dark matter + dark energy) from many alternative theories of gravity. This idea has already been applied in the context of DGP and  $f(R)$  gravity for which specific CMB-galaxy cross-correlation signatures at high redshifts have been predicted by the authors of [21, 22].

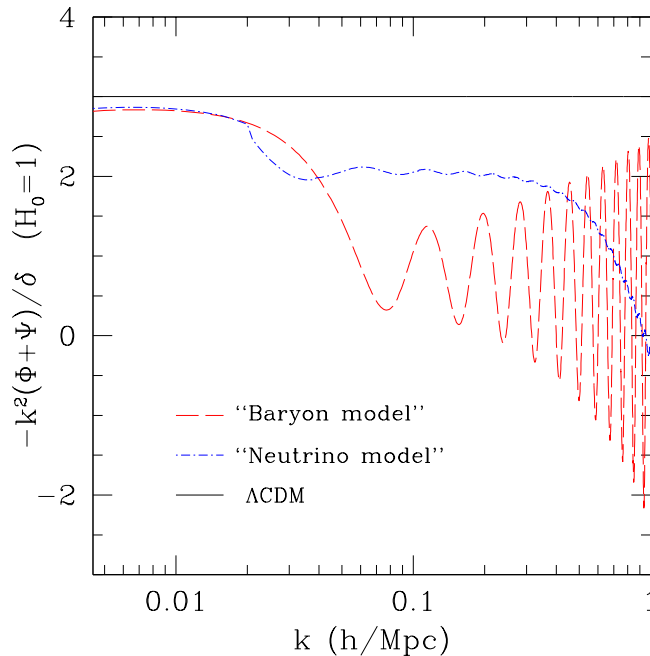


FIG. 1: The “poisson ratio”  $-k^2(\Phi + \Psi)/(\Omega_b\delta_b + \Omega_\nu\delta_\nu)$  for the two TeVeS models considered in section III. In these units, the Poisson ratio is constant and equal to 3 in standard  $\Lambda$ CDM cosmology (solid line). This is true in TeVeS only for the largest scales, where the standard term in the Poisson equation dominates. On smaller scales the vector field perturbations dominate and the Poisson ratio exhibits a much more complicated behavior (see §III for more details).

## II. INTEGRATED SACHS-WOLFE EFFECT

A CMB photon traveling through time-varying gravitational potentials  $\Phi$  and  $\Psi$  in the metric (1) will suffer a change in energy, resulting in a change in the observed CMB temperature: the so-called Integrated Sachs-Wolfe (ISW) effect. The fractional change in CMB temperature in the direction  $\hat{\mathbf{n}}$  is given by an integral along the line of sight back to the redshift of last scattering:

$$\frac{\Delta T(\hat{\mathbf{n}})}{T} = \int_0^{z^{\text{LSS}}} dz \frac{d}{dz} (\Phi(\mathbf{r}, z) + \Psi(\mathbf{r}, z))|_{\mathbf{r}=\chi(z)\hat{\mathbf{n}}} \quad (2)$$

where  $\chi(z)$  is the comoving distance out to redshift  $z$ . The evolution of the gravitational potentials therefore determines the ISW effect. On the other hand, the fractional overdensity of galaxies along the line of sight is

$$\delta_g(\hat{\mathbf{n}}) = \int_0^\infty dz W(z) \delta_g(\chi(z)\hat{\mathbf{n}}; z) \quad (3)$$

where  $W(z)$  is the redshift distribution of galaxies (normalized so it integrates to unity), determined both by the intrinsic redshift distribution of galaxies and by the properties of the survey at hand.

Since we expect an overdensity of galaxies to be correlated with potential wells, we expect a non-zero correlation between the observed temperature anisotropy and the observed angular galaxy distribution. This correlation is however model-dependent and can be used to distinguish between different theories of gravity.

If we focus on large scales, the fractional galaxy overdensity in Fourier space is

$$\delta_g(\mathbf{k}, z) = b(z)\delta(\mathbf{k}, z=0)D(k, z) \quad (4)$$

where  $b(z)$  is the time-dependent but scale-independent bias, and  $D(k, z)$  is the linear growth function, normalized to unity today. In standard  $\Lambda$ CDM, the growth function depends on  $z$  only, but more generally (and in TeVeS in particular) it can have a scale dependence. With this restriction to large angular scales, the angular cross-power spectrum at a multipole  $l$  is

$$C_{gT}(l) = \frac{2}{\pi} \int_0^\infty dk k^2 P(k) \delta_g(l, k) \delta_{\text{ISW}}(l, k) \quad (5)$$

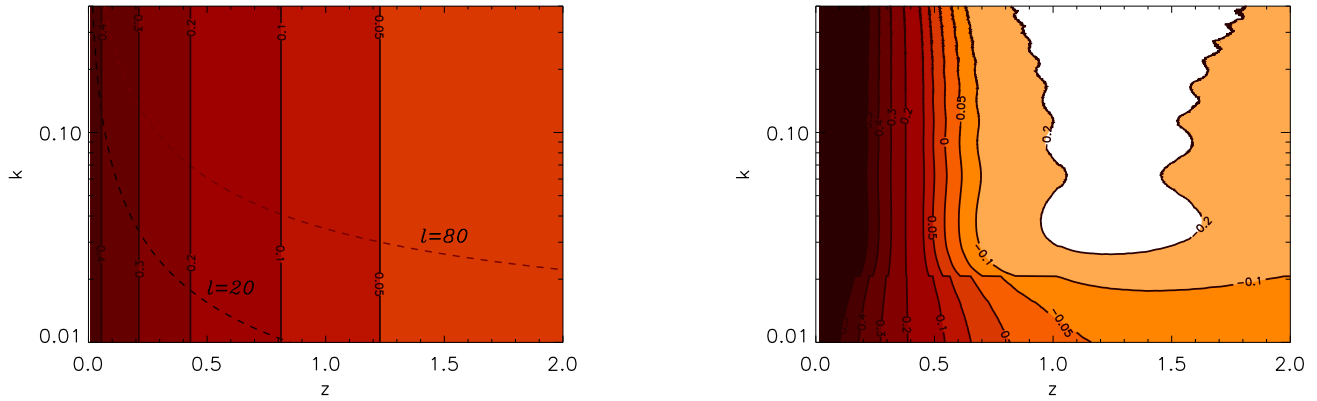


FIG. 2: *Left Panel.*  $k^2 D_{\text{ISW}}/H_0^2$  as a function of wavenumber  $k$  and redshift in standard  $\Lambda\text{CDM}$ . Here we show results from linear theory so the relevant growth functions do not depend on wavenumber. Dashed curves show the line along which the integral is performed for two values of  $l$ . *Right panel.*  $k^2 D_{\text{ISW}}/H_0^2$  as a function of wavenumber  $k$  and redshift in TeVeS. Note that at high redshift, the TeVeS weighting function goes negative.

where  $P(k)$  is the matter power spectrum today, and the two weighting functions for galaxies and the ISW effect are:

$$\delta_g(l, k) = \int_0^\infty dz W(z) b(z) D(z, k) j_l(k \chi(z)) \quad (6)$$

$$\delta_{\text{ISW}}(l, k) = \int_0^{z_{\text{LSS}}} dz \frac{d}{dz} \left( -\frac{\Phi(k, z) + \Psi(k, z)}{\delta(k, z=0)} \right) \cdot j_l(k \chi(z)) \equiv \int_0^{z_{\text{LSS}}} dz D_{\text{ISW}}(k, z) j_l(k \chi(z)) \quad (7)$$

Here,  $\delta_g(l, k)$  gives the contribution of the modes with wave number  $k$  to the projected overdensity of galaxies for the spherical harmonic  $l$  and  $j_l$  is the spherical Bessel function.

We then use the Limber approximation (valid for  $l \gtrsim 10$  and an arbitrary smooth function  $f(k)$ ):

$$\int dk k^2 f(k) j_l(k \chi) j_l(k \chi') \rightarrow \frac{\pi}{2} \frac{1}{\chi^2} f(k = (l + 1/2)/\chi) \delta_{\text{Dirac}}(\chi - \chi') \quad (8)$$

This simplifies the expression for the galaxy-CMB cross-power coefficients to a single integral (we set  $c = 1$ ):

$$C_{gT}(l) = \int dz \frac{H_0(z)}{\chi^2(z)} D(z, k_\perp) b(z) W(z) D_{\text{ISW}}(k_\perp, z) P(k_\perp), \quad k_\perp \equiv \frac{l + 1/2}{\chi(z)}. \quad (9)$$

The galaxy-CMB angular correlation function  $w_{gT}(\theta)$  can be calculated in a similar way [23]:

$$w_{gT}(\theta) = \frac{1}{2\pi} \int dk k P(k) \int_0^\infty dz b(z) W(z) D(k, z) D_{\text{ISW}}(k, z) J_0(k \chi(z) \theta) \quad (10)$$

Here,  $J_0$  denotes the Bessel function of order zero.

Equation (9) states that the  $C_{gT}(l)$  are determined by a weighted integral of  $D_{\text{ISW}}(k, z)$  along the line  $k = (l + 1/2)/\chi(z)$  in the  $(k, z)$ -plane. The function  $D_{\text{ISW}}$  defined in equation (7) represents the response of the potentials to the growth of matter overdensities. In the case of standard  $\Lambda\text{CDM}$ , it is given by the Poisson equation:

$$k^2 \Phi = -\frac{3}{2} H_0^2 \Omega_m (1+z) \delta(k, z), \quad \text{and } \Psi = \Phi \Rightarrow D_{\text{ISW}}(k, z) = -\frac{3}{k^2} H_0^2 \Omega_m \frac{d}{dz} (1+z) D(z) \quad (11)$$

The left panel of Fig. 2 shows  $D_{\text{ISW}}$  as a function of  $k$  and  $z$  in the standard  $\Lambda\text{CDM}$  model and the right panel for TeVeS. The dashed curves in the left panel show the line along which the integral is performed in  $(k, z)$  space for two values of  $l$ . Larger values of  $l$  probe smaller scales and therefore higher  $k$ -values. At low  $z$ , the two theories make similar predictions (the larger amplitude for TeVeS at low redshift is model-dependent), whereas the differences become large for redshifts larger than one.

The striking differences in between the two panels in Fig. 2 are due to the differences in the growth of structure in TeVeS and standard  $\Lambda\text{CDM}$  during the matter dominated era. In absence of cold dark matter, the growth factor

in TeVeS must be enhanced with respect to  $\Lambda$ CDM in order to match the present amplitude of perturbations. This enhancement produces an evolution of the gravitational potential, and thus an ISW signal during matter domination. This does not happen in  $\Lambda$ CDM, where the ISW contribution comes *only* from the decay of the potential during dark energy domination.

At redshifts of order one,  $D_{\text{ISW}}$  even becomes negative for TeVeS, leading to negative cross-power. For large  $z$  samples, this feature of TeVeS should have observable consequences. Before examining these consequences, we explain the features of TeVeS that lead to the behavior depicted in Fig. 2, in the following section.

### III. THE GENERALIZED POISSON EQUATION IN TEVES

Perturbations around the smooth cosmology in TeVeS were first studied in [10] with the full set of evolution equations derived in [11]. The equations which determine the scalar potentials of equation (1) are [11]:

$$-2k^2\bar{\Phi} - 2e^{4\bar{\phi}}\frac{\dot{b}}{b}\left(3\dot{\bar{\Phi}} + k^2\zeta + 3\frac{\dot{b}}{b}\bar{\Psi}\right) = K_B k^2 E + 8\pi G a^2 \bar{\rho} \delta \quad (12)$$

$$\dot{\bar{\Phi}} + \frac{\dot{b}}{b}\bar{\Psi} = 4\pi G a^2 e^{-4\bar{\phi}}(\rho + P)\Theta \quad (13)$$

where  $\bar{\phi}$  is the zero order smooth part of the TeVeS scalar field;  $b \equiv ae^{\bar{\phi}}$ ;  $\alpha$  and  $E$  characterize perturbations to the vector field;  $\bar{\rho}$  is the background matter density;  $\Theta$  is proportional to the velocity of the matter;

$$\zeta \equiv (e^{-4\bar{\phi}} - 1)\alpha; \quad (14)$$

and  $K_B$  is a dimensionless parameter governing the importance of the vector field. Here we have neglected the scalar field perturbations as these are small.

In the following we will assume matter domination, including baryons and massive neutrinos (no cold dark matter). Using equation (13) we can write the term in parenthesis in equation (12) as:

$$\left(3\dot{\bar{\Phi}} + k^2\zeta + 3\frac{\dot{b}}{b}\bar{\Psi}\right) = 12\pi G a^2 e^{-4\bar{\phi}}(\rho + P)\Theta + k^2\zeta. \quad (15)$$

On sub-horizon scales we can neglect the  $\Theta$  term. Then, using the definition of  $\zeta$  and  $\frac{\dot{b}}{b} = \frac{\dot{a}}{a} + \dot{\bar{\phi}}$ , we obtain the generalized Poisson equation:

$$\bar{\Phi} = -\frac{3H_0^2(\Omega_b\delta_b + \Omega_\nu\delta_\nu)}{2ak^2} - \frac{K_B E}{2} - \left(\frac{\dot{a}}{a} + \dot{\bar{\phi}}\right)(1 - e^{4\bar{\phi}})\alpha. \quad (16)$$

The first term on the right is the standard contribution from matter, but the last two are unique to TeVeS. Perturbations to the vector field affect the behavior of the gravitational potential, destroying the simple 1-1 relationship between potential and density implicit in general relativity.

To get an equation for the other scalar potential, we use the relation [11]:

$$\bar{\Psi} = \bar{\Phi} + e^{4\bar{\phi}}\left[\dot{\zeta} + 2\left(\frac{\dot{a}}{a} + 2\dot{\bar{\phi}}\right)\zeta\right]. \quad (17)$$

From equation (14) we get:

$$\dot{\zeta} = -4\dot{\bar{\Phi}}e^{-4\bar{\phi}}\alpha + (e^{-4\bar{\phi}} - 1)\dot{\alpha}. \quad (18)$$

The evolution equation for  $\alpha$  is:

$$\dot{\alpha} = E + \bar{\Psi} + \left(\dot{\bar{\phi}} - \frac{\dot{a}}{a}\right)\alpha, \quad (19)$$

hence:

$$\dot{\zeta} = -4\dot{\bar{\Phi}}e^{-4\bar{\phi}}\alpha + (e^{-4\bar{\phi}} - 1)E + (e^{-4\bar{\phi}} - 1)\bar{\Psi} + (e^{-4\bar{\phi}} - 1)\left(\dot{\bar{\phi}} - \frac{\dot{a}}{a}\right)\alpha. \quad (20)$$

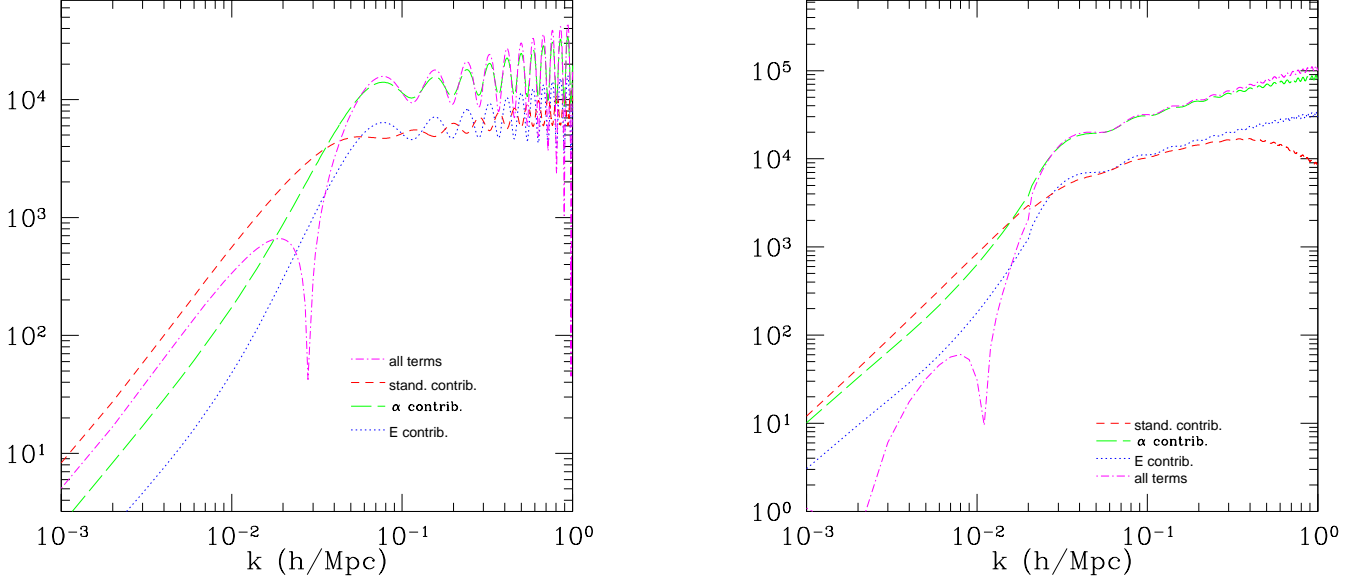


FIG. 3: *Left Panel.*  $|k^2\Phi|$  in the TeVeS baryon model (see text). After integrating numerically the TeVeS perturbation equations we plot the output for  $|k^2\Phi|$  and the different contributions to  $|k^2\Phi|$  from the other perturbation variables, according to the Poisson equation. In the plot, “standard contrib.” is the standard  $\delta$  term on the R.H.S. of the Poisson equation, “ $\alpha$  contrib.” represents the  $\left(\frac{\dot{a}}{a} + \dot{\bar{\phi}}\right) (1 - e^{4\bar{\phi}}) \alpha$  term and “E contrib.” is the  $K_B E/2$  term (all these terms have been multiplied by  $k^2$ ). “All terms” is the sum of all the R.H.S. terms. On the x-axis  $k$  is in units of h/Mpc but plotted lines correspond to units in which  $H_0 = 1$ . Same for all the following plots. *Right panel.* Same curves, but in the TeVeS neutrino model.

We can now include these expressions into equation (17) to get, after some algebra:

$$\Psi = e^{-4\bar{\phi}}\Phi + (e^{-4\bar{\phi}} - 1)E + \left[\frac{\dot{a}}{a}(e^{-4\bar{\phi}} - 1) + \dot{\bar{\phi}}(e^{-4\bar{\phi}} - 5)\right]\alpha. \quad (21)$$

Using the Poisson equation (16) leads to:

$$\Psi = -\frac{3e^{-4\bar{\phi}}H_0^2(\Omega_b\delta_b + \Omega_\nu\delta_\nu)}{2ak^2} + \left[e^{-4\bar{\phi}}\left(1 - \frac{K_B}{2}\right) - 1\right]E - 4\dot{\bar{\phi}}\alpha. \quad (22)$$

Again the first term on the right is familiar from general relativity but the vector field perturbations induce two new source terms. Summing  $\Phi$  and  $\Psi$ , we obtain:

$$\begin{aligned} \Phi + \Psi &= -\frac{3H_0^2}{2k^2}(\Omega_b\delta_b + \Omega_\nu\delta_\nu)(1 + e^{-4\bar{\phi}}) + \left[-\frac{K_B}{2}(1 + e^{-4\bar{\phi}}) + e^{-4\bar{\phi}} - 1\right]E - \left[\left(\frac{\dot{a}}{a} + \dot{\bar{\phi}}\right)(1 - e^{-4\bar{\phi}}) + 4\dot{\bar{\phi}}\right]\alpha \\ \xrightarrow{\bar{\phi} \ll 1} &-3\frac{H_0^2}{k^2}(\Omega_b\delta_b + \Omega_\nu\delta_\nu) - \frac{K_B}{2}E + 4\dot{\bar{\phi}}\alpha \end{aligned} \quad (23)$$

The limit  $\bar{\phi} \ll 1$  is imposed by nucleosynthesis bounds on  $\Omega_{\bar{\phi}}$  [10].

Equation (23) can significantly differ from the Poisson equation in standard cosmology (equation (11)) if the vector field perturbations  $\alpha$  and  $E$  are large. Two of us [12] showed that  $\alpha$  and  $E$  get large when  $K_B \rightarrow 0$ . Thus we expect the Newtonian potentials  $\Phi$  and  $\Psi$  to deviate from standard Poisson expectations in this strong TeVeS regime. We also see that, unlike the standard term, the vector field terms in the TeVeS Poisson equation do not decrease as  $1/k^2$ . This suggests that the corrections might actually dominate on small scales.

We solved the full set of evolution equations in two different models. The first (called “baryon model” in the following), has only baryons with  $\Omega_b = 0.3$  and  $K_B = 0.08$ ; the second (“neutrino model”) has massive neutrinos with  $\Omega_\nu = 0.17$ ,  $\Omega_b = 0.05$ ,  $K_B = 0.08$ . The left panel of Fig. 3 shows the contributions to  $|k^2\Phi|$  given by the different terms in equation 16 for the baryon model. The right panel shows the same for the neutrino model. In both cases we can see that the standard term  $-3e^{-4\bar{\phi}}H_0^2(\Omega_M\delta_M)/2ak^2$  dominates on large scales but it becomes basically negligible on small scales, where the  $\alpha$  contribution is the dominant one. An analogous result is obtained for  $|k^2\Psi|$  (Fig. 4) but this time the dominant contribution on small scales is produced by the vector perturbation variable  $E$  instead of  $\alpha$ .

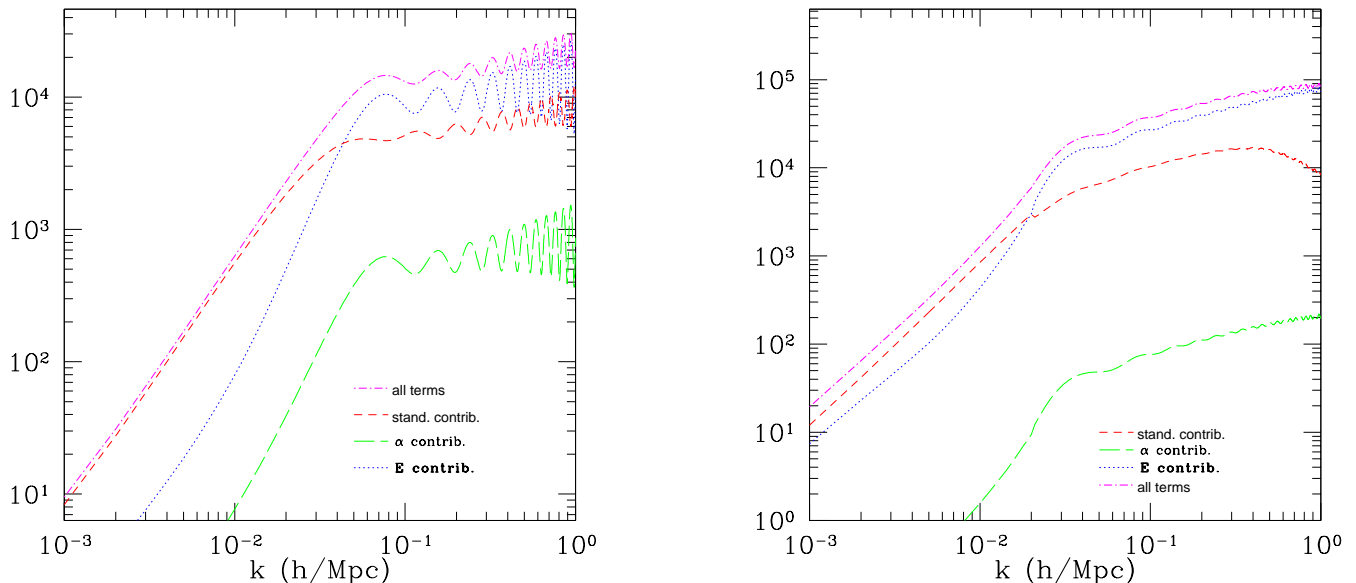


FIG. 4: *Left Panel.*  $|k^2\Psi|$  in the TeVeS baryon model. After integrating numerically the TeVeS perturbation equations we plot the output for  $|k^2\Psi|$  and the different contributions to  $|k^2\Phi|$  from the other perturbation variables, according to the equation (22). *Right panel.* Same curves, but in the TeVeS neutrino model.

In Fig. 1 we showed the “Poisson ratio”  $-k^2(\Phi + \Psi)/(\Omega_b\delta_b + \Omega_\nu\delta_\nu)$ . In a standard cosmological model this quantity is a constant but in TeVeS this is no longer true on small scales, where the vector field contributions in the Poisson equation dominate. In the baryon model the Poisson ratio shows large oscillations on small scales. The reason for this can be understood by looking at Fig. 3 and 4. When we consider the Poisson ratio on small scales we are basically dividing  $\alpha$  and  $E$  (green and blue lines in the figures) by  $\delta$  (“standard contrib.,” red line). We see that the acoustic oscillations in  $\alpha$  and  $E$  are much more pronounced than and out of phase with those in  $\delta$ . This produces the large oscillations that are finally observed. Acoustic oscillations are generated by the baryon component, which is much smaller in the neutrino model. This also explains why we do not see oscillations in the neutrino model Poisson ratio. Another feature of the neutrino model Poisson ratio is a decreasing trend on small scales (dashed-dotted blue line in Fig. 1). This is due to neutrinos entering the free streaming regime and thus producing a decay in  $\delta$  (red line in the right panels of Fig. 3 and 4) not matched by a corresponding decay in  $E$  and  $\alpha$ .

Finally, Fig. 5 (left panel) shows the effect of the vector field on the matter power spectrum. In this figure we considered our baryon model with  $\Omega_b = 0.3$  and we changed the value of  $K_B$  while keeping the other TeVeS parameters fixed as usual. We know that the effect of reducing  $K_B$  is to boost the growth of vector perturbations and to enhance the growth factor of matter perturbations as well (see [12]). We also see that reducing  $K_B$  shifts the peak of the power spectrum to smaller scales.

#### IV. RESULTS

The authors of [10] showed that a flat TeVeS model with  $\Omega_\nu = 0.17$ ,  $\Omega_b = 0.05$ ,  $\Omega_\Lambda = 0.78$  (i.e. the “neutrino model” we considered in the previous section) can produce a galaxy power spectrum in reasonable agreement with present observations. This means that a direct measurement of the power spectrum from galaxies is not the best discriminator of the TeVeS model and standard  $\Lambda$ CDM cosmology. It is then worthwhile to ask whether there are other large scale structure observables that can be used to distinguish between TeVeS and standard  $\Lambda$ CDM, even in the case of similar predicted power spectra.

We know that in order to match a  $\Lambda$ CDM power spectrum without resorting to a CDM component, TeVeS needs a substantial contribution from the vector field perturbations  $E$  and  $\alpha$ . As shown in the previous section, this leads to important modifications in the Poisson equation. These modifications are in turn responsible for the change in  $D_{ISW}$  with respect to standard GR illustrated in Fig. 2 and can thus potentially produce an observable effect in the galaxy-CMB cross correlation given by equation (9) and (10). Note that since the TeVeS model contains a dark energy component, we also expect a *late time* ISW effect similar to that in the standard  $\Lambda$ CDM scenario when this

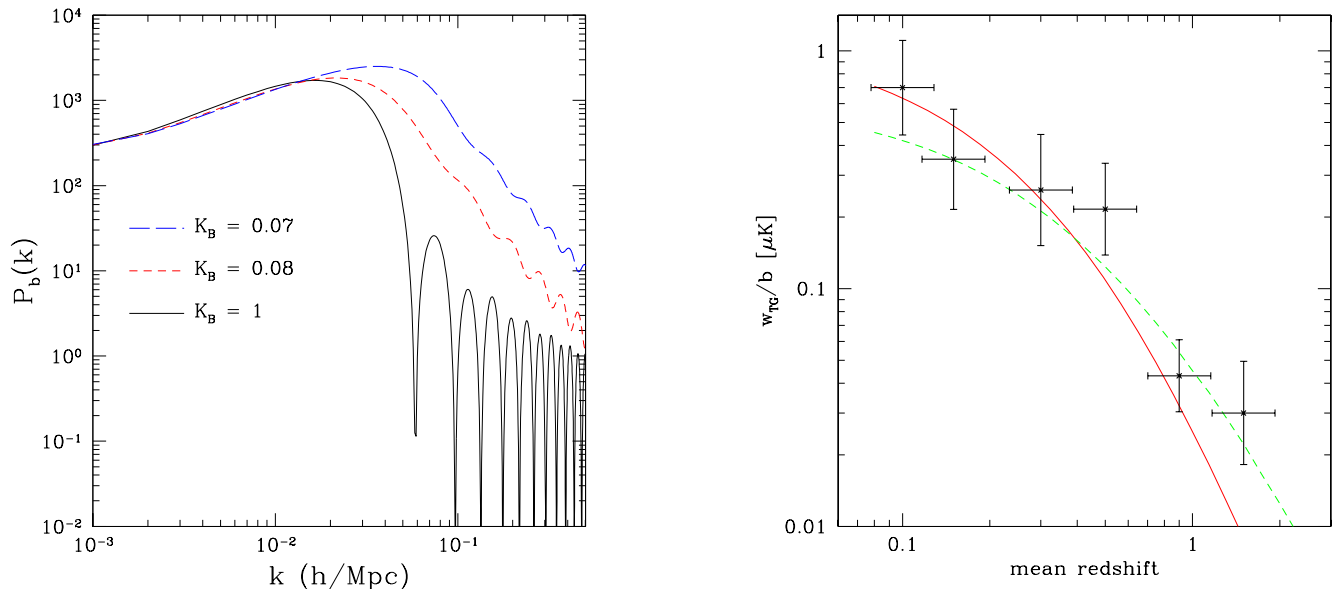


FIG. 5: *Left panel:* Matter power spectra for a TeVeS baryon only model with fixed  $\Omega_b = 0.3$  and different values of  $K_B$ . *Right panel:* Galaxy-CMB cross correlation function at  $\theta = 6^\circ$  (divided by the galaxy bias) from different surveys [23, 24]. The red (solid) curve shows the TeVeS neutrino model prediction, while the green (dashed) curve is the  $\Lambda\text{CDM}$  prediction.

component starts to dominate.

For the following calculations, we use the  $\Lambda\text{CDM}$  linear power spectrum calculated using the transfer function from [25] for both TeVeS and  $\Lambda\text{CDM}$ , as it is accurate to the percent level, whereas the power spectrum in the TeVeS framework is not yet known to the desired degree of precision. Throughout, we assume the following parameters for the  $\Lambda\text{CDM}$  cosmology:  $h = 0.7$ ,  $\Omega_m = 0.27$ ,  $\Omega_\Lambda = 0.73$ ,  $\Omega_b = 0.046$ ,  $\sigma_8 = 0.8$ ,  $n_s = 0.95$ .

So far, the ISW effect has been detected in the cross-correlation of the CMB with galaxy surveys in the radio, infrared, optical, and X-ray bands (see [23] for a summary of recent results). These detections span a redshift range from 0.1 to 0.9. Recently, a cross-correlation with the SDSS quasar catalog has been performed [24] which has a median redshift of 1.5. Fig. 5 (right panel) shows the different observational results in terms of the angular cross-correlation function evaluated at  $\theta = 6^\circ$ . Also shown are predictions from the TeVeS neutrino model and the  $\Lambda\text{CDM}$  cosmology defined above. In order to evaluate equation (10), we assumed a  $z$ -dependent galaxy selection function according to equation (12) in [23].

Clearly, the low- $z$  (late-time) ISW effect predicted by TeVeS is quite similar to that of  $\Lambda\text{CDM}$  and consistent with the current observations. The effects of the TeVeS vector fields become noticeable only beyond  $z = 1$ , where there are no strong constraints yet.

In order to determine whether future surveys will be able to distinguish the TeVeS scenario from  $\Lambda\text{CDM}$ , we adopt a fiducial survey (“Sample 1” in Ref. [26]) with parameters expected from the future Large Synoptic Survey Telescope (LSST, [27]): we assume a galaxy sample with a limiting magnitude of 27 in the I band and a sky coverage of  $f_s = 0.5$ . Dividing the survey into several redshift bins, the observed number of galaxies per arcmin<sup>2</sup> as a function of redshift for each bin,  $W(z)$ , is then given by the observed  $z$ -dependent luminosity function of galaxies [28, 29] convolved with a smoothed top hat redshift window (Eq. (16) in [26]). This roughly takes into account the scatter expected in the photometric redshifts. The mean redshifts of galaxies in the four bins considered range from 0.49 up to 3.54. In order to convert from galaxy overdensity to matter overdensity, we have to assume a mean galaxy bias in each redshift

	Bin 1	Bin 2	Bin 3	Bin 4
$\langle z \rangle$	0.49	1.93	2.74	3.54
$b$	1.08	2.02	2.90	3.89
$n_g$	34.6	10.1	3.89	1.68

TABLE I: Parameters of the four redshift bins for the assumed LSST-like survey [26].  $\langle z \rangle$  is the average redshift of galaxies in the bin,  $b$  is the mean galaxy bias, and  $n_g$  is the observed number of galaxies per arcmin<sup>2</sup> in each redshift bin.

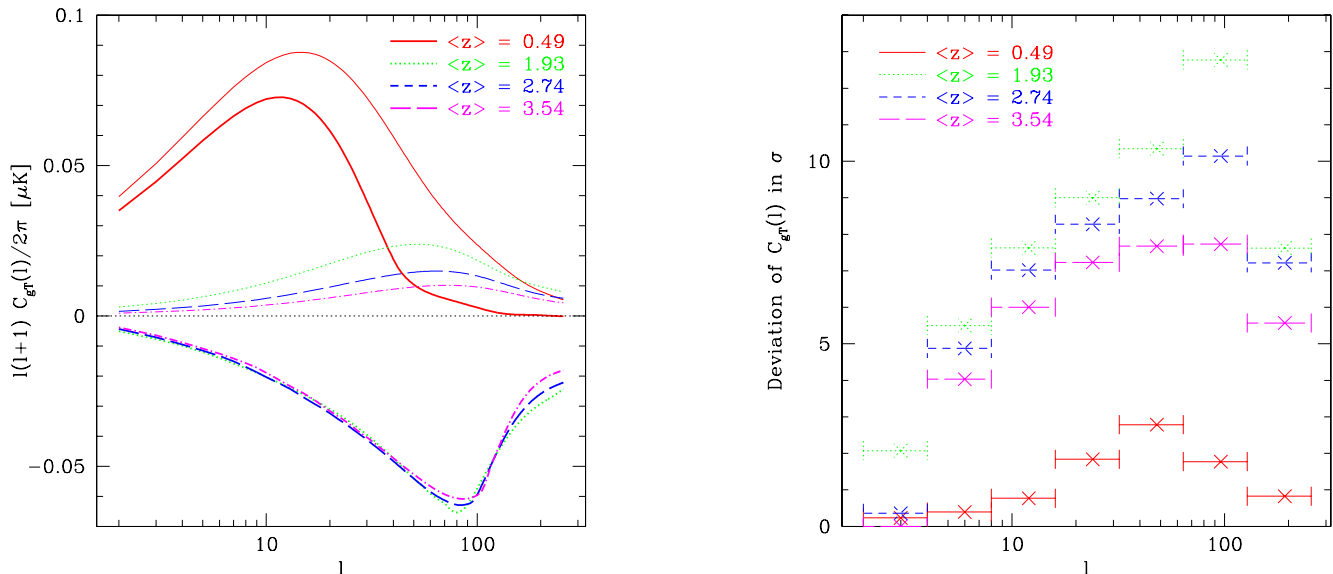


FIG. 6: *Left panel:* The cross-correlation of galaxies and the CMB for a LSST-like galaxy survey and four redshift bins, in TeVeS (thick lines) and GR ( $\Lambda\text{CDM}$ , thin lines). *Right panel:* The significance of the TeVeS–GR deviation in the galaxy–CMB cross power for the LSST-like survey; i.e. difference between TeVeS and GR divided by the expected error in each angular bin.

bin. This was calculated in [26] using the halo occupation distribution and the halo mass function from simulations [30, 31]. In actual surveys, the bias is determined from the data itself. The characteristics of the redshift bins are summarized in Tab. I. With these parameters, we can evaluate equation (9). Note that we neglect the magnification bias [26] as well as redshift errors here. These effects are not expected to affect our main conclusions.

Fig. 6 (left panel) shows the cross-power spectra for TeVeS (thick lines) and  $\Lambda\text{CDM}$  (thin lines) for the different redshift bins. As expected, the TeVeS cross-power is similar to  $\Lambda\text{CDM}$  in the lowest redshift bin and goes negative at high  $z$  (the “baryon model” considered above shows the same qualitative behavior). To estimate the detectability of this effect, we bin the cross-power spectra in  $l$ , taking the errors on a given multipole moment as:

$$(\Delta C_{gT})^2(l) = \frac{1}{f_s(2l+1)} \left( C_{gT}^2(l) + C_{TT}(l)(C_{gg}(l) + \frac{1}{n_g}) \right), \quad (24)$$

where  $C_{gT}$  is the galaxy–temperature cross-correlation;  $C_{TT}$  and  $C_{gg}$  are the CMB and galaxy auto-power spectra respectively; and  $n_g$  is the number density of galaxies per sr (so that  $4\pi f_s n_g$  is the total number of galaxies in the corresponding redshift bin of the survey; see Tab. I). Throughout we set  $f_s = 0.5$ , and errors on different  $C_{gT}(l)$  are assumed to be uncorrelated. Fig. 6 (left panel) then shows the difference between the adopted  $\Lambda\text{CDM}$  model and TeVeS divided by the expected error in each angular bin. The TeVeS predictions are clearly distinguishable from the  $\Lambda\text{CDM}$  model, reaching significances of over  $10\sigma$  in the high redshift bins. In addition, the negative sign of the correlation at high  $z$  is an unambiguous signature of this modified gravity theory.

## V. SUMMARY AND CONCLUSIONS

TeVS is a modified gravity theory originally introduced by Bekenstein [9] with the purpose of providing a covariant relativistic framework for Milgrom’s paradigm of Modified Newtonian Dynamics (MOND). Further investigations [10] showed that a TeVeS model with massive neutrinos and no cold dark matter component can pass some fundamental cosmological tests. In particular, it was shown that such a model can reproduce observations of the CMB and galaxy power spectra.

In light of these results, in this paper we raised the following question: are there cosmological observables that are able to clearly distinguish between TeVeS and standard  $\Lambda\text{CDM}$ ?

In order to reproduce a  $\Lambda\text{CDM}$  power spectrum without using cold dark matter, TeVeS has to incorporate a mechanism to enhance the standard growth rate of perturbations [12]. This in turn produces a characteristic ISW signature detectable in principle by looking at the CMB–galaxy cross-correlation. In section II we computed the ISW

effect in TeVeS, showing that the characteristic quantity  $D_{ISW}(k, z)$  presents clear differences between TeVeS and  $\Lambda$ CDM at intermediate redshifts  $z \gtrsim 1$ . By deriving the generalized Poisson equation in the TeVeS framework (Section III) we showed that the same vector field perturbations that are responsible for the growth of large scale structure in TeVeS are also the cause for the different predictions for the ISW effect.

The TeVeS model studied here is consistent with current observations of the ISW effect (Fig. 5, right panel) which reach up to  $z \approx 1.5$ . In order to determine whether the TeVeS predictions are constrainable in future surveys, we computed the expected CMB-galaxy cross-correlation for a fiducial survey with parameters expected from the future LSST (Section IV). Our results show that at high redshifts ( $z \gtrsim 2$ ), TeVeS and  $\Lambda$ CDM will be clearly distinguishable, with significances of over  $10\sigma$ . Moreover we found that the sign of the CMB-galaxy cross-correlation at high redshifts differs between TeVeS and  $\Lambda$ CDM, thus providing a smoking-gun signature for this kind of modified gravity. We emphasize that this CMB-galaxy *anti-correlation* at high redshifts is a robust prediction, since it is due to the additional degrees of freedom that are necessary for large scale structure to form in a TeVeS cosmology.

We would finally like to stress that our work was conducted in the framework of TeVeS because this provides a well-defined test model for which the evolution of linear perturbations has already been studied. However, as pointed out by Bertschinger [20], the characteristic TeVeS features that give rise to the studied effect are expected to be common to a large class of modified gravity models. Thus we expect the CMB-galaxy cross-correlation to be a general and powerful tool to discriminate among many alternative modified gravity theories.

### Acknowledgments

We would like to thank Pengjie Zhang for useful discussions. This work was supported by the DOE at Fermilab and by the Kavli Institute for Cosmological Physics at the University of Chicago through grants NSF PHY-0114422 and NSF PHY-0551142 and an endowment from the Kavli Foundation and its founder Fred Kavli. ML was supported by PPARC.

- 
- [1] S. M. Carroll et al., Phys. Rev. **D71**, 063513 (2005), astro-ph/0410031.
  - [2] D. A. Easson, Int. J. Mod. Phys. **A19**, 5343 (2004), astro-ph/0411209.
  - [3] G. Cognola, E. Elizalde, S. Nojiri, S. D. Odintsov, and S. Zerbini, JCAP **0502**, 010 (2005), hep-th/0501096.
  - [4] R. P. Woodard (2006), astro-ph/0601672.
  - [5] S. Carloni, P. K. S. Dunsby, S. Capozziello, and A. Troisi, Class. Quant. Grav. **22**, 4839 (2005), gr-qc/0410046.
  - [6] M. Amarguoui, O. Elgaroy, D. F. Mota, and T. Multamäki, Astron. Astrophys. **454**, 707 (2006), astro-ph/0510519.
  - [7] S. Nojiri and S. D. Odintsov (2006), hep-th/0601213.
  - [8] M. Milgrom, Astrophys. J. **270**, 371 (1983).
  - [9] J. D. Bekenstein, Physical Review **D70**, 083509 (2004).
  - [10] C. Skordis, D. F. Mota, P. G. Ferreira, and C. Boehm, Phys. Rev. Lett. **96**, 011301 (2006), astro-ph/0505519.
  - [11] C. Skordis, Phys. Rev. **D74**, 103513 (2006), astro-ph/0511591.
  - [12] S. Dodelson and M. Liguori, Phys. Rev. Lett. **97**, 231301 (2006), astro-ph/0608602.
  - [13] F. Bourliot, P. G. Ferreira, D. F. Mota, and C. Skordis (2006), astro-ph/0611255.
  - [14] A. Lue and G. D. Starkman, Phys. Rev. Lett. **92**, 131102 (2004), astro-ph/0310005.
  - [15] P. Zhang, M. Liguori, R. Bean, and S. Dodelson (2007), arXiv:0704.1932 [astro-ph].
  - [16] R. Scranton et al. (SDSS) (2003), astro-ph/0307335.
  - [17] N. Afshordi, Y.-S. Loh, and M. A. Strauss, Phys. Rev. **D69**, 083524 (2004), astro-ph/0308260.
  - [18] P. Fosalba, E. Gaztanaga, and F. Castander, Astrophys. J. **597**, L89 (2003), astro-ph/0307249.
  - [19] N. Padmanabhan et al., Phys. Rev. **D72**, 043525 (2005), astro-ph/0410360.
  - [20] E. Bertschinger, Astrophys. J. **648**, 797 (2006), astro-ph/0604485.
  - [21] Y.-S. Song, I. Sawicki, and W. Hu, Phys. Rev. **D75**, 064003 (2007), astro-ph/0606286.
  - [22] P. Zhang, Phys. Rev. **D73**, 123504 (2006), astro-ph/0511218.
  - [23] E. Gaztañaga, M. Manera, and T. Multamäki, Mon. Not. R. Astron. Soc. **365**, 171 (2006), arXiv:astro-ph/0407022.
  - [24] T. Giannantonio, R. G. Crittenden, R. C. Nichol, R. Scranton, G. T. Richards, A. D. Myers, R. J. Brunner, A. G. Gray, A. J. Connolly, and D. P. Schneider, Phys. Rev. D **74**, 063520 (2006), arXiv:astro-ph/0607572.
  - [25] D. J. Eisenstein and W. Hu, Astrophys. J. **496**, 605 (1998), arXiv:astro-ph/9709112.
  - [26] M. LoVerde, L. Hui, and E. Gaztanaga, Phys. Rev. **D75**, 043519 (2007), astro-ph/0611539.
  - [27] H. Zhan, L. Knox, J. A. Tyson, and V. Margoniner, Astrophys. J. **640**, 8 (2006), arXiv:astro-ph/0508119.
  - [28] A. Gabasch, R. Bender, S. Seitz, U. Hopp, R. P. Saglia, G. Feulner, J. Snigula, N. Drory, I. Appenzeller, J. Heidt, et al., Astron. Astrophys. **421**, 41 (2004), arXiv:astro-ph/0403535.
  - [29] A. Gabasch, U. Hopp, G. Feulner, R. Bender, S. Seitz, R. P. Saglia, J. Snigula, N. Drory, I. Appenzeller, J. Heidt, et al., Astron. Astrophys. **448**, 101 (2006), arXiv:astro-ph/0510339.

- [30] A. V. Kravtsov, A. A. Berlind, R. H. Wechsler, A. A. Klypin, S. Gottlöber, B. Allgood, and J. R. Primack, *Astrophys. J.* **609**, 35 (2004), arXiv:astro-ph/0308519.
- [31] R. K. Sheth and G. Tormen, *Mon. Not. R. Astron. Soc.* **308**, 119 (1999), arXiv:astro-ph/9901122.